Spring 5-12-2017

MOLECULARLY TARGETED NANOMEDICINE: ROLE OF HSP90 INHIBITOR AND SOPHOROLIPIDS IN THE TREATMENT OF LUNG CANCER

Shuguftha Naz Ms
Pittsburg State University, nshuguftha@gus.pittstate.edu

MOLECULARLY TARGETED NANOMEDICINE: ROLE OF HSP90 INHIBITOR AND SOPHOROLIPIDS IN THE TREATMENT OF LUNG CANCER

A thesis submitted to the Graduate School
In Partial Fulfillment of the Requirements
For the Degree of
Master of Science in Polymer Chemistry

Shuguftha Naz

Pittsburg State University

Pittsburg, Kansas

May 2017

MOLECULARLY TARGETED NANOMEDICINE: ROLE OF HSP90 INHIBITOR AND SOPHOROLIPIDS IN THE TREATMENT OF LUNG CANCER

Shuguftha Naz

APPROVED:

Thesis Advisor _____
Dr. Santimukul Santra, Department of Chemistry

Committee Member _____
Dr. Khamis Siam, Department of Chemistry

Committee Member _____
Dr. Irene Zegar, Department of Chemistry

Committee Member _____
Dr. Jian Hong, Kansas Polymer Research Center

ACKNOWLEDGMENTS

I take this opportunity to express my deep gratitude to Almighty Allah and my Parents who guided me all throughout my life.

I am indebted and do feel highly elated in manifesting a deep sense of gratitude to my guide, Dr. Santimukul Santra for his constant support and encouragement. I owe to him for guiding me the right path all way in personal and professional life and allowing me to expose our research at conferences and made me to learn and share others research.

I am grateful to Dr. Tuhina Banerjee for her unwavering support during the entire course of the projects. She helped us in understanding the mechanisms and assays which were very crucial for our projects. My sincere thanks to her for making us what we are today and for being like a mother when we need them.

My deepest thanks to my committee members, Dr. Khamis Siam, Dr. Irene Zegar and Dr. Jian Hong for turning out this thesis to be successful. They helped me in various phases either directly or indirectly and made me a good person.

I would like to thank Department of Chair, Dr. Petar Dvornic for his constant encouragement and support all throughout the course.

I express my heartfelt thanks to Dr. William Shirley, Dr. McAfee, Dr. Ram Gupta, Dr. Dilip Paul, Dr. Jody Neef and Dr. Kristopher Mijares for the friendly nature and their time given to us. They created the environment of healthy discussion and fun, which made me more confident.

I am also greatly thankful to Dr. Virgina Rider for providing us with cell culture facility and allowing us to work day and night without any interruption.

I extend my thanks to Pittsburg State University for giving me this opportunity to study and do research at the time of need which changed my life. Very thankful to Chemistry department and Dr. Santra again!

I thank Kansas Soybean Commission from bottom of my heart because of whom I got graduate assistance ship with Dr. Santra. The topical lotion project with KSC is one of the finest projects of my life. Thanks to all associated with it.

It is a pleasure to thank my fellow mates of lab, Jyothi Kallu, Shoukath Sulthana, Tyler Shelby, Blaze Heckert, Riyadh Alnasser, Tanuja Tummala and my friends, Fayaz Mohammed, Iliyas Ahmed and Shaik Ashfaq.

I owe my deepest gratitude to my brother, Late. Mohammad Sameer and my sister, Neha Naz for their constant encouragement and supporting me all throughout my life.

Last but not the least; I thank my parents, because of whom I am here and for being what I am. They supported and guided me in every phase of difficulty and happiness and made me the person what I am today. I would also like to thank my love, Mohammed Sumair Ahmed for his encouragement and support.

I offer my regards and blessings to all of those who supported me in any respect during the completion of the project. I extend my sincere thanks to my well-wishers.

I whole-heartedly thank all those who have stretched their helping hands towards me directly or indirectly for successful completion of this thesis. I extend my sincere thanks to all.

MOLECULARLY TARGETED NANOMEDICINE: ROLE OF HSP90 INHIBITOR AND SOPHOROLIPIDS IN THE TREATMENT OF LUNG CANCER

An Abstract of the Thesis by
Shuguftha Naz

Lactonic sophorolipids (LSL) are a class of enzymatically modified glycolipids known to have HDAC inhibition activity and anticancer properties. Ganetespib (GT), an Hsp90 inhibitor, is known for its superior antitumor activity in several K-RAS mutant Non-Small-Cell Lung Cancer (NSCLC) cells. In this study, a new anti-oxidant nanoplatform is formulated using the combination of these two drugs, LSL and GT, in order to target both HDAC inhibition and Hsp90 signaling pathways in NSCLC. Nanoceria (NC) is an excellent redox platform will be specifically used to supplement the therapeutic potency of these drugs in the effective treatment of NSCLC. We hypothesized that the therapeutic efficacy of GT will be synergistically accelerated by the HDAC inhibition and redox activity of LSL and NC, respectively. For this, polyacrylic acid-coated nanoceria (NC-COOH) is synthesized using solvent precipitation method and folic acid is conjugated using ‘click’ chemistry in order to target NSCLC and to minimize adverse side effects. As a result of combination therapy, enhanced ROS production is detected and more than 80% reduction in the cell viability is recorded within 24 h of incubation. Migration assays indicated that the highly metastatic nature of NSCLC is successfully restricted upon treatment of these drugs-loaded functional nanoceria. In addition, various cell-based assays including detection of apoptosis and necrosis, HDAC inhibition, MTT and fluorescence microscopy are performed to validate the highly effective combination therapy of NSCLC. Together, our results represent for a unique combination of drugs and personalized delivery system for the effective treatment of K-RAS driven undruggable NSCLC.

TABLE OF CONTENTS

LIST OF FIGURES

LIST OF SCHEMES

LIST OF ABBREVIATIONS

HAT	Histone acetylases
HDAC	Histone deacetylases
LSL	Lactonic Sophorolipid
MDR	Multi-drug resistance
NSCLC	Non-small-cell lung cancer
K-RAS	Kristen rat sarcoma
GT	Ganetespib
NC	Nanoceria (cerium oxide nanoparticles)
ROS	Reactive oxygen species
EDC	1-Ethyl-3-(3-dimethylaminopropyl) carbodiimide
NHS	(N-hydroxysuccinimide)
MES	2-(*N*-morpholino) ethanesulfonic acid
EE	Encapsulation efficiency
FT-IR	Fourier transform infrared spectroscopy
DLS	Dynamic light scattering
MTT	3-(4,5-dimethylthiazol-2-yl)-2,5-diphenyltetrazolium bromide
CHO	Chinese Hamster Ovarian cells
FITC	Fluorescein isothiocyanate
FBS	Foetal bovine serum
DMF	Dimethyl formamide
DMSO	N, N'-dimethyl sulfoxide
DHE	Dihydroethidium

CHAPTER I

Introduction

Histone acetylation and deacetylation plays a crucial role in the regulation of gene expression.[1] They are balanced by two most important enzymes histone acetylases (HAT) and histone deacetylases (HDAC).[2-4] Altered expression and mutation of genes associated with HDAC are directly linked to cell proliferation and tumor development.[5,6] Studies have shown that HDAC inhibitors are known to alter gene expression and influence on cellular growth arrest, cytotoxicity and induce apoptosis.[7-12] Thus, the development of HDAC inhibitors, their therapeutic role and mechanism of action has received tremendous attention in the field of cancer treatment.[13,14] Lactonic sophorolipid (LSL) is a glycolipid molecule synthesized from specific yeast species.[15,16] Many reports are available on the immunomodulatory and anti-inflammatory properties of LSL.[17-20] However, studies have reported on the anticancer activity of LSL on different cell lines including pancreatic, esophageal and lung cancer.[18-26] It is indicated that one of the mechanisms for anti-tumor activity of LSL is the HDAC inhibition, where the histone deacetylases are inhibited and interferes with the gene expression.[17]

Lung carcinomas are currently the leading cause of cancer-related mortality worldwide due to its poor prognosis, multidrug resistance (MDR) and low survival rate.[27-29] Approximately, more than 85% of lung cancer cases are related to non-

small-cell lung cancer (NSCLC) and the major histopathological subtypes are adenocarcinomas, squamous cell carcinomas and large cell carcinomas.[28,30-34] Oncogenic K-RAS mutations in human NSCLC (10-30%) have gained resistance to chemotherapy and radiation.[35-37] Although K-RAS mutations are well known, yet there is a lack of effective therapeutic options available for K-RAS driven NSCLC.[35] Severe side effects, multidrug resistance and poor survival outcomes are the limitations of current NSCLC therapies,[38,39] and this is indicative of the urgency in the development of an effective chemotherapy for the treatment of NSCLC.

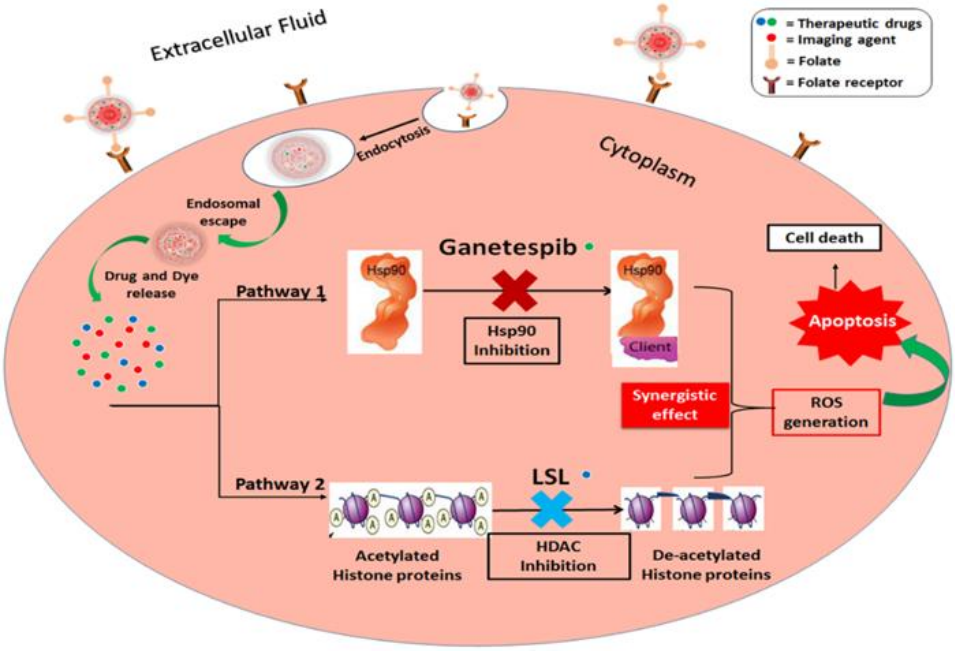

Figure 1: Schematic representation of the mechanism of actions of the combination of drugs: ganetespib and lactonic sophorolipid for the effective treatment of NSCLC.

Targeted delivery of two or more chemotherapeutic drugs specifically to tumor site is becoming a popular choice for the effective treatment of cancer. The combination therapy allows inhibition of separate tumorigenesis pathways that overcomes severe side effects, multidrug resistance, and have potential to improve treatment response. Considering the importance of combination therapy, a new drug combination, ganetespib (GT) and LSL is proposed in this study. We reasoned that GT is a second generation Hsp90 inhibitor, which leads to the degradation of major client proteins. It disrupts important signaling cascades responsible for cell proliferation and survival of tumor.[40-43] GT is also known to have potential antineoplastic activity and shown promising results in the treatment of NSCLC in past few years.[42,44-47] In addition, the use of nanotechnology-based drug delivery system has become an emerging area of interest for better payloads, biocompatibility and targeted delivery of chemotherapeutic drugs, which resulted in minimal side effects.[48-53] Recent studies indicated the huge potential of various nanoparticles as drug carriers in cancer therapy, including targeted drug delivery, diagnosis, imaging, and treatment.[31,54-57] Among others, cerium oxide nanoparticles (NC) has received considerable attention due to its excellent catalytic and anti-oxidant properties on different cell systems.[58-62] As an antioxidant, many reports are available indicating its cytotoxic nature towards cancer cells, whereas protective effects in certain neurodegenerative disorders.[63]

Herein, we report an innovative combination therapy approach for the effective treatment of NSCLC (A549 cells). Blend of chemotherapeutic drugs, LSL and GT, are encapsulated into the folate-conjugated nanoceria, which minimizes the off-

target effects of drug combinations. Additionally, the anti-oxidative nature of nanoceria facilitates for the survival of healthy tissues, while *in situ* generation of chronic oxidative stress in the tumor cells reduces its viability. This property of NC supplements the synergistic therapeutic actions, where LSL plays an important role in HDAC inhibition and GT inhibits the Hsp90 signaling pathways towards the treatment of NSCLC (**Figure 1**).[64,65] The therapeutic effects of this combination therapy are examined by performing various cell-based assays including cell viability, enhanced ROS, apoptosis and necrosis, migration and HDAC assays. Taken together, findings from this study would provide clinically acceptable strong support for the NSCLC treatment decision making and potential translational applications of the nanomedicine.

CHAPTER II

Results and Discussion

Synthesis and Characterizations of poly (acrylic acid) (PAA)-coated Cerium Oxide Nanoparticles (PNC):

Previously reported water-based alkaline precipitation method was used to synthesize polyacyrilic acid coated nanoceria (NC-COOH).[66] The obtained yellow color solution of nanoceria was centrifuged to get rid of agglomerates and bigger size particles and was further purified by dialysis technique (MWCO 6-8 kDa) **(1, Scheme 1).**[67] Optical lipophilic DiI dye was encapsulated in NC-COOH (encapsulation efficiency, EE_{DiI} = 85%) using modified solvent diffusion method. DiI dye is important for optical imaging because of its high extinction coefficient (ε > 125000 cm^{-1} M^{-1}) and higher fluorescence emission (λ_{max} = 585 nm) and used as negative optical probe to evaluate the toxicity of carboxylated nanoceria. To functionalize our nanoparticles, carboxylic acid groups of NC-COOH (2 X 10^{-3} mol) were conjugated with propargylamine (15 X 10^{-3} mol) using EDC (15 X 10^{-3} mol) and NHS (15 X 10^{-3} mol) chemistry in the presence of MES buffer (pH = 6.0). In presence of CuI catalyst, using click chemistry, folic acid was conjugated on the surface of nanoparticles to target lung cancer expressing folate receptors on the surface **(4 and 5, Scheme 1).** Click chemistry is the reaction between folate-azide (2 X 10^{-2} mol) and triple bond of propargylamine (1.5 X 10^{-3} mol). The prepared folate nanoceria was further purified using dialysis technique and then encapsulated with DiI dye via solvent diffusion

method, which is used as positive control for targeted delivery of drugs. Encapsulation of therapeutic drugs, LSL and GT in folate nanoceria **(5, Scheme 1, 1.0 X 10^{-3} mol, $EE_{LSL/GT}$ = 75%)** using same modified solvent diffusion method was done for therapeutic applications. Finally, these preparations were dialyzed for purification and stored at 4° C for further characterizations.

Characterizations of PAA Polymer-Coated Functional Nanoceria.

The synthesized NC-COOH was characterized by FT-IR spectroscopy **(Figure 2)** to confirm the presence of carboxyl groups on the surface as an indication of successful coating of polyacyrilic acid. The presence of a carboxyl stretching band at 1685 cm^{-1} confirmed the presence of C = O stretching indicating the successful coating of PAA polymer on nanoceria. PAA coating makes our nanoparticle sable, compatible and allows efficient encapsulation of drugs. The carboxyl groups on the surface allow conjugation of various functional groups for targeted delivery. Dynamic light scattering studies showed the presence of monodisperse nanoceria preparation with an average hydrodynamic diameter of 56.75 ± 2 nm **(Figure 2B)**. The overall surface charge of the different functional nanoceria preparations was assessed by ζ potential and was found to be -25.6 mV for NC-COOH and -11.8 mV for NC-FOL. **(Figure 3A and 3B)**.

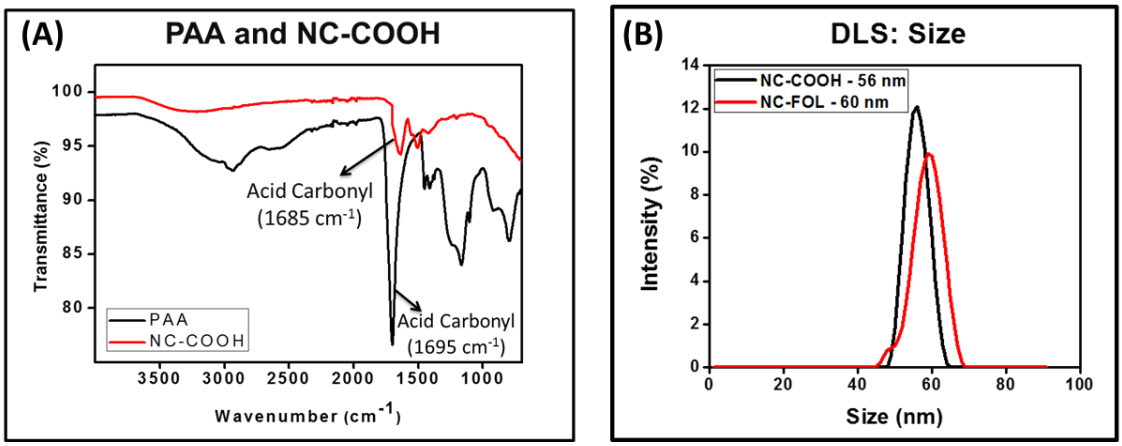

Figure 2: The presence of PAA coating in NC was confirmed by the presence of acid carbonyl band at 1685 cm-1 in FT-IR spectrum. Determination of the size of NPs using dynamic light scattering (DLS) showing the average hydrodynamic diameter of 56.75 nm. Conjugation of folic acid on the surface of nanoceria and successful encapsulation of optical DiI dye in the polymer coating was confirmed by UV-Vis absorbance and fluorescence spectroscopy using a high–throughput plate reader. The absorbance spectrum of DiI encapsulating folate nanoceria **(Figure 3E)** confirmed the presence of both DiI dye (λ_{abs} = 585 nm) and folic acid (λ_{abs} = 360 nm). This was further confirmed by their corresponding fluorescence spectra (FoI: λ_{em} = 460 nm; DiI: λ_{em} = 600 nm, **Figure 3D and 3F**). The size and fluorescence of these nanoceria preparations were remained to be unchanged for longer duration indicating the stable synthesis of nanoceria.

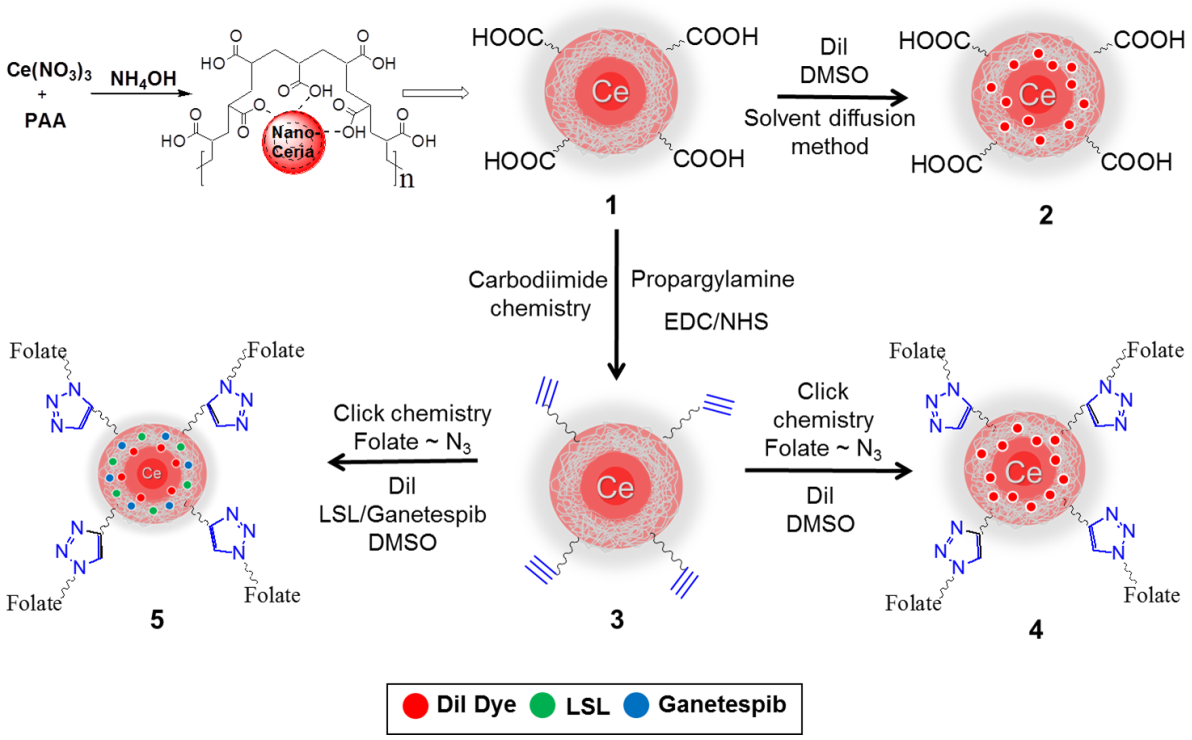

Scheme 1: Schematic representation of redox cerium oxide nanoparticles. **(1)** Nanoceria was synthesized using alkaline precipitation method with PAA coating on its surface. **(3)** Propargylated NPs were synthesized using carbodiimide chemistry. Click chemistry has been used to functionalize the NPs with folic acid **(4 and 5).** Co-encapsulation of dye and chemotherapeutic drugs was done using solvent diffusion method **(2, 4 and 5)** to produce desired functional NPs.

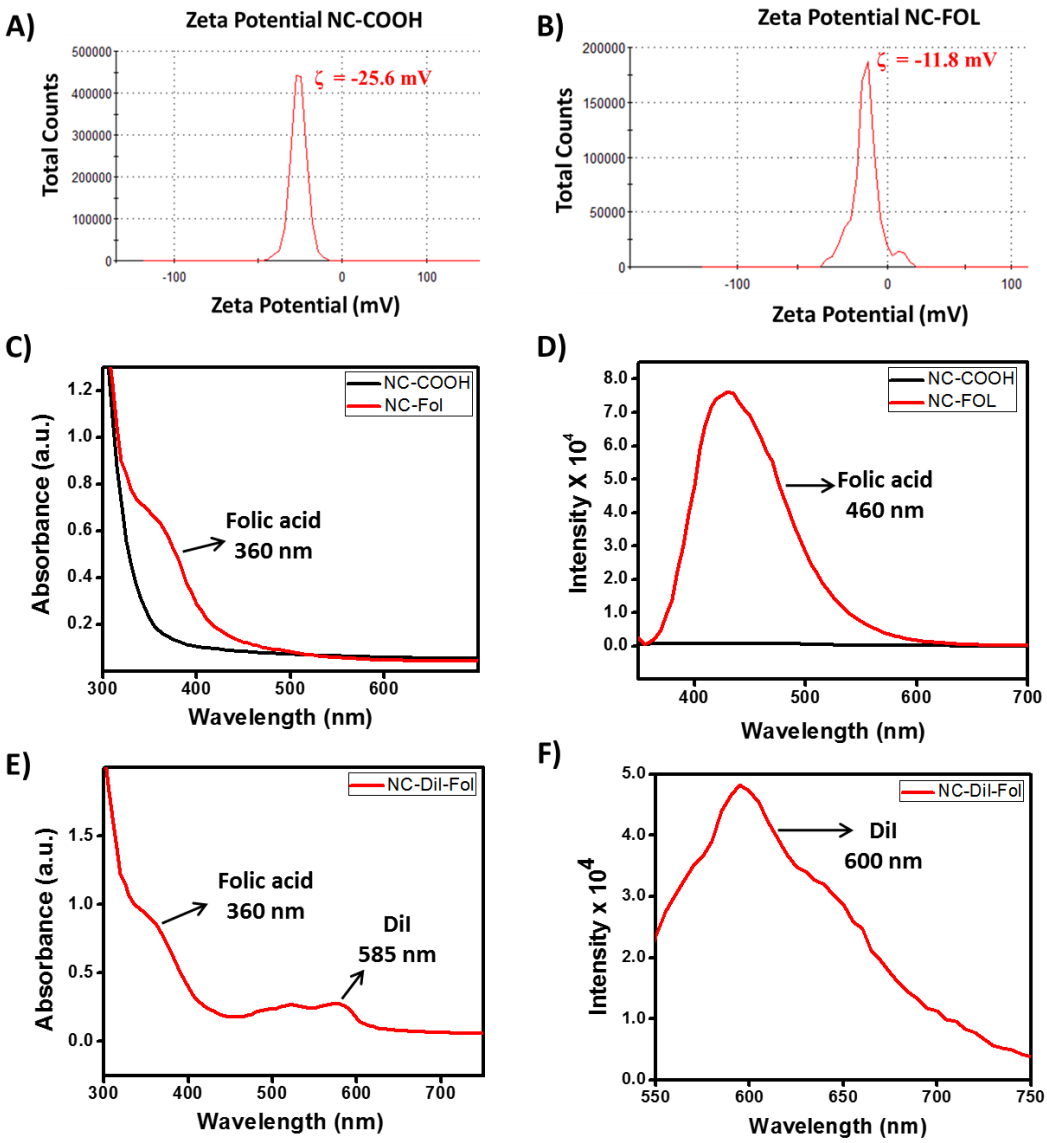

Figure 3: Characterization of functional nanoceria. **(A and B)** Average zeta potential (surface charge) of NC-COOH and NC-FOL was found to be -25.6 and -11.8 mV by DLS. **(C)** UV-Visible absorption spectra at 360 nm and **(D)** Fluorescence emission spectra at 460 nm confirms the successful conjugation of folic acid on the surface of the NPs. **(E)** Presence of folic acid and DiI dye is confirmed by the UV absorption bands at 360 nm and 585 nm. **(F)** Fluorescence emission spectra of NPs encapsulated with DiI dye (λmax = 600 nm).

Drug release profiles:

To verify the drug release kinetics of our nanoparticle in the presence of appropriate external environment, we determined the release profile of the drug and dye from the nanocarrier at two different pH conditions (acidic – 6.0 and physiological – 7.4) *in vitro*. According to hypothesis, the polymer coatings of nanoparticles are disrupted in acidic environment thereby releasing the cargos. Time dependent study of released cargos was determined using the plate reader.

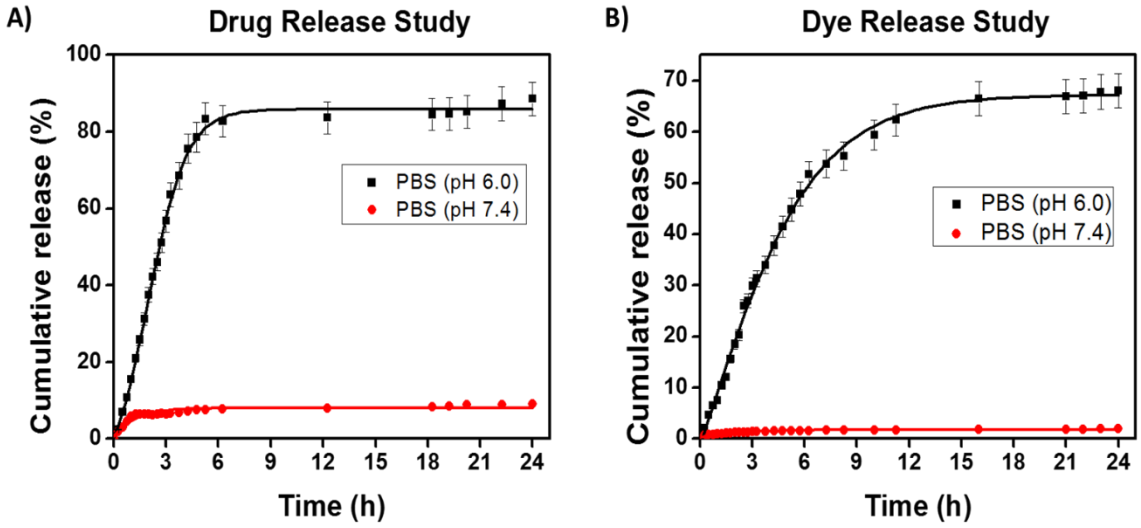

Figure 4: Controlled drug release profiles of NC-LSL-FOL using dialysis method. **(A)** Controlled release of LSL drug from encapsulated NPs with time in acidic pH (pH 6.0) was observed and about 80% of drug is released within 6 h of time. However, minimal release was seen at normal pH (pH 7.4). **(B)** Similarly, release of DiI dye in acidic pH was studied at (λ_{em} = 585 nm) using UV where the absorption maxima increase with release of time. However, there is no or minimal release of drug and dye at normal pH conditions.

In the cumulative release of drug at pH 6.0 as shown in **Figure 4A**, a burst release of drug (80%) was observed within 6 h and then the release was stable. Whereas, the dye

release was slower when compared to that of the drug. Maximum amount of dye was released in 12 h of time (60%) and then remained stable **(Figure 4B)**. In contrast, at physiological pH, no detectable release of drug or dye was observed. These results confirm that our nanoparticles release the cargos within the acidic environment of tumor cells and are stable at normal pH.

Cell viability assay (MTT Assay):

In an attempt to assess the therapeutic efficacy of nanoceria loaded with cargos, a series of cytotoxic experiments were conducted with different functional nanoparticles on two different cell lines, A549 (folate-positive) and CHO (folate-negative) cells in a time dependent manner. Briefly, cells (2500 cells/well) were seeded in 96-well plate and incubated with various functional folate conjugated nanoceria preparations (35 µL, 1.0 X 10^{-3} mol) at 37°C followed by incubation of MTT. The data was collected at regular intervals of time. Interestingly, upon incubation with LSL alone more than 40 % of cells were found to be dead after 24 h of incubation. This was synergized by GT and both the drugs in combination (NC-LSL-GT-FOL, 1.0 X 10^{-3} mol) showed more than 80% of cell death within 24 h of incubation and when continued to 48 h, it showed 90% of cell death **(Figure 5A)**. However, nanoceria by itself without drugs showed minimal toxicity to both the cancer cells and normal cells, indicating the biocompatibility of our redox-based drug delivery system. No significant cytotoxicity was observed when CHO cells were incubated with drug loaded folate nanoceria (**Figure 5B)** due to the absence of folate receptors. The main characteristic of our nanoplatform is to minimize the side effects and increase the uptake of drugs via active targeting by using folate conjugated nanoceria. From the results, it is evident that LSL activity is accelerated by GT as result of synergistic effect.

Thus, the targeted delivery of our functional nanoceria encapsulated with LSL and GT would provide an excellent therapy for potentially addressing the MDR effect in the treatment of undruggable NSCLC and other tumors.

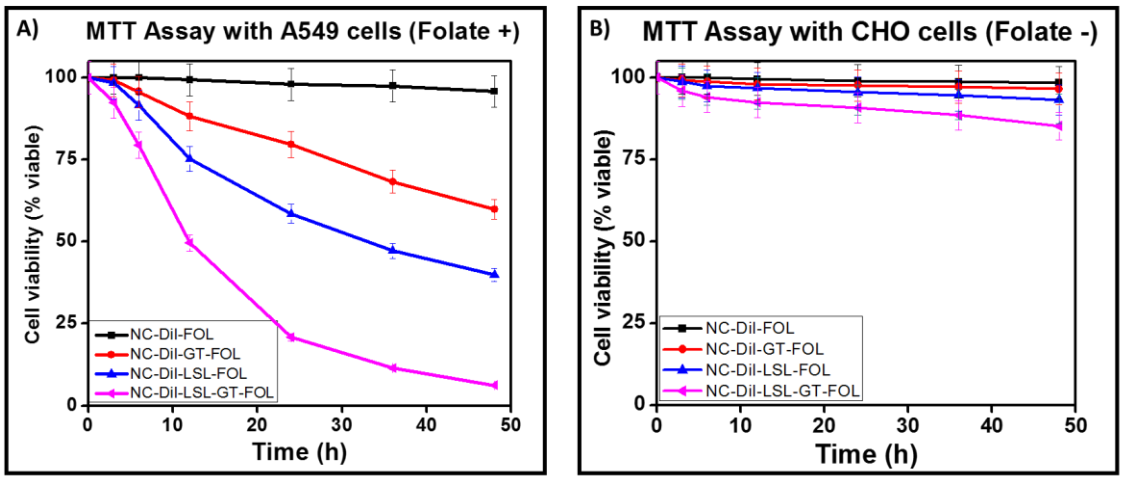

Figure 5: Determination of cytotoxicity of formulated nanoceria using MTT assay. (A) More than 80% of cells were dead within 24 h when incubated combinational drugs carrying nanoceria, whereas only 40% toxicity was observed with delivery of single drug. (B) On the other hand, minimal toxicity was observed when functional nanoceria was incubated with CHO cells (FR -), suggesting targeted delivery of drugs specifically to tumor site.

Confocal Laser-Scanning Microscopy:

To shed light on dye release monitoring in living cells, we recorded a set of laser scanning fluorescent microscopic images to visualize the intracellular dye and drug release. During the imaging process, to avoid heat effect-induced cell death the exposure time of laser was given shorter than 400 ms. We hypothesized that folate conjugated nanoceria would target tumors overexpressing folate receptors and gets internalized, minimizing the toxicity to healthy cells. When carboxylated nanoceria encapsulated with combinational

drugs (NC-LSL-GT-COOH, 1.0 X 10^{-3} mol, **Figure 6A-6D**) was incubated in A549 cells, there was no or minimal internalization. This is due to the lack of folate ligands on the surface of our nanoparticle which could not target folate receptors. According to our hypothesis, folate conjugated nanoceria will gets internalized in the folate expressing tumors. To validate this, A549 cells were incubated with folate nanoceria encapsulated with DiI dye and interestingly, internalization of nanoceria with the release of dye was observed as the cytoplasm was found to be red (**Figure 6E-6H)**. To further demonstrate the folate receptor-mediated internalizations, A549 cells were incubated with LSL and GT loaded folate nanoceria (1.0 X 10^{-3} mol) huge change in cellular morphology was observed where the cytoplasm is ruptured and the nucleus is disorganized **(Figure 6I-6L)**. These results signify the local targeting and delivery of drugs effectively to cancer cells. When CHO cells were incubated with drugs encapsulating folate nanoceria, there was no or minimal internalization due to the lack of folate receptors on the surface of CHO cells (Healthy cells). This confirms the tumor-targeting ability of our functional nanoceria, while minimizing the toxicity to healthy cells. **(Figure 6M-6P).** Taken together, these results indicate the possibility of our designed nanoplatform to be used for targeted delivery in clinical trials.

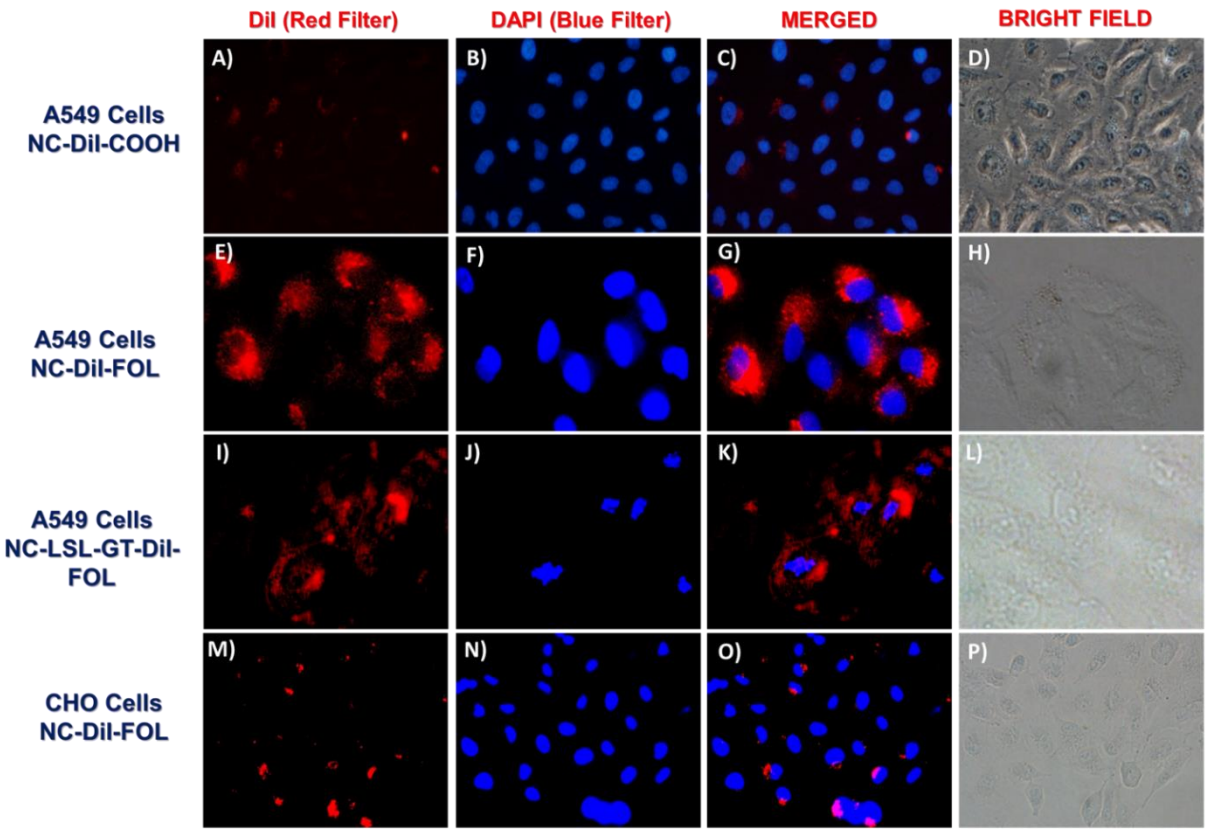

Figure 6: Representative fluorescence microscopic images of the in vitro cellular imaging and drug delivery experiments. No or minimal internalization of carboxylated NPs loaded with combination of drugs was observed in A549 cells due to absence of folic acid on surface of NPs **(A-D)**. Effective internalization of folate NPs with no drugs was observed due to folate receptor-mediated endocytosis **(E-F)**. However, when drugs-loaded folate nanoceria was incubated with A549 cells, substantial amount of cell death was observed **(I-L)**. In contrast, minimal internalization of folate NPs was observed in CHO cells due to the absence of folate receptors on the surface of the CHO cells **(M-P)**, indicating the targeted drug delivery. Nucleus stained with DAPI dye (blue).

Cytosolic ROS detection assay:

A newer approach to achieve better anticancer therapy is to enhance ROS levels selectively in the cancer cells. The generation of ROS in the cell is determined by Dihydroethidium (DHE), a fluorescent dye which is oxidized to 2-hydroxyethidium in the presence of reactive oxygen species and gives red fluorescence after intercalating within the nuclei. Previous studies have shown ROS generation via HDAC inhibition as one of the mechanisms by which LSL exerts its antitumor activity. To determine the GT synergizes the ROS production of LSL, A549 cells were treated with combinational drugs, LSL and GT carrying folate nanoceria (**5,** 1.0 X 10^{-3} mol, **Scheme 1**). Briefly, A549 cells were seeded into 12-well plates (10000 cells/well) and when confluent, they are incubated with different functional nanocarriers: (1) folate nanoceria without drug (NC-FOL), (2) folate nanoceria with GT alone (NC-GT-FOL), (3) folate nanoceria with only LSL (NC-LSL-FOL), (4) folate nanoceria with combinational drugs (NC-LSL-GT-FOL). After 6 h of treatment of drugs, the cells were washed and stained with cytosolic cell permeable probe dihydroethidium (DHE) for 30 min. As expected, the cells treated with folate nanoceria showed minimal fluorescence due to limited ROS stress (**Figure 7A-i)**. Folate nanoceria with GT showed significant amount of fluorescence indicating the stress induced by ROS (**Figure 7C-iii)**. In contrast, folate nanoceria encapsulated with only LSL showed elevated ROS levels as observed by higher fluorescence intensity (**Figure 7B-ii).** This is due to the cytotoxicity of LSL via HDAC inhibition pathway. When incubated with combinational drugs **(**NC-LSL-GT-FOL, 1.0 X 10^{-3} mol, **5, Scheme 1**)**,** there was huge rise in the levels of ROS **Figure 7D-iv** and this validates that the synergistic effect of GT improves therapeutic efficacy of LSL by trigerring ROS generation.

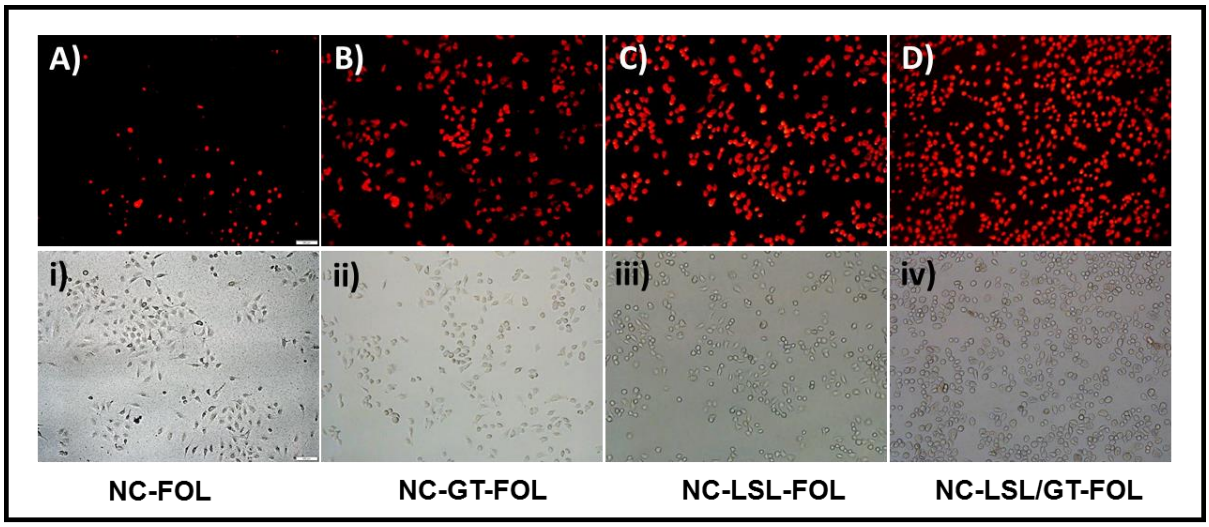

Figure 7: Determination of ROS generation. Incubation of A549 cells with different nanocarriers shows the increase in fluorescence due to increased ROS levels. Due to the effect of synergism, ROS levels are increased in order of folate nanoceria to folate nanoceria with combinational drugs.

In addition, quantification of ROS was determined by calculating the numerical data of fluorescence intensities from each fluorescence microscopic images using commercial ImageJ software and the graph was plotted as shown in **Figure 8.**

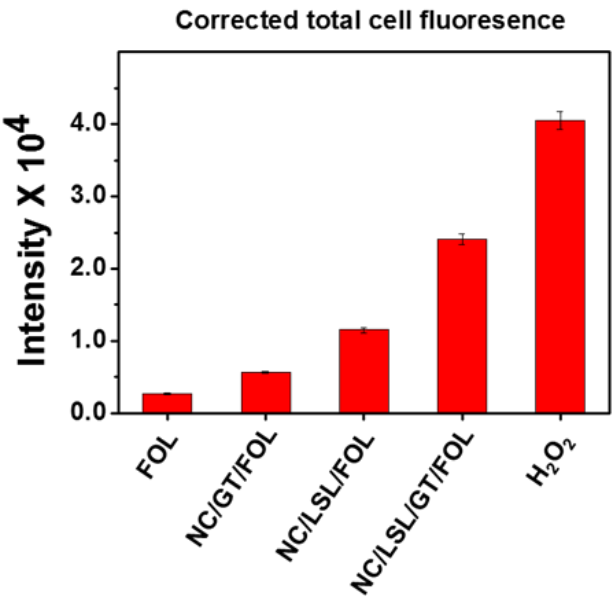

Figure 8: Quantification of ROS: Amount of ROS generation was quantified directly from the microscopic images using Image J software. Results showed relatively higher fluorescence from A549 cells treated with combinational drugs due to the presence of increased amount of ROS.

Apoptosis and necrosis detection assay:

Increased ROS production is incriminated in apoptosis and has been reported as an early event which is followed by necrosis. Having known that our functional nanoceria produces ROS, next we want to further elucidate the correlation between ROS generation and apoptosis induction. In these experiments, A549 cells were exposed to various nanocarriers, NC-FOL, NC-GT-FOL, NC-LSL-FOL and NC-LSL-GT-FOL (1.0×10^{-3} mol) for 24 h. In our study, the apoptotic and necrotic cells were distinguished on the basis of their cell integrity and morphology by using fluorescence microscope. Upon staining with Annexin V-FITC and Ethidium homodimer III, the apoptotic and necrotic cells exhibited green and red fluorescence respectively. This is due to the various morphological and biochemical changes occurring the tumor cells including the translocation of

phosphatidylserine (PS) due to apoptosis. As demonstrated in the **Figure 9A,** folate nanoceria shows fewer apoptotic cells which is related to the antioxidant nature of nanoceria. Annexin V and ethidium homodimer staining pattern determines that NC-LSL-FOL leads to early and late apoptosis (major green spots for apoptotic cells and fewer red spots for necrotic cells, **(Figure 9C)**. Upon treatment with combinational drugs, increased apoptotic and necrotic cells were seen **(Figure 9D)** thus confirming that treatment of GT accelerates the LSL apoptosis induction leading to extensive loss in membrane integrity, eventually leading to cell death via necrosis. Taken together, our results suggest that combination of LSL and GT might provide better anti-tumor effect through synergistic effect in the treatment of NSCLC. In addition, the development of functional nanoceria encapsulated with combinational drugs would be an ideal drug delivery system for targeted combination therapy of NSCLC and other tumors.

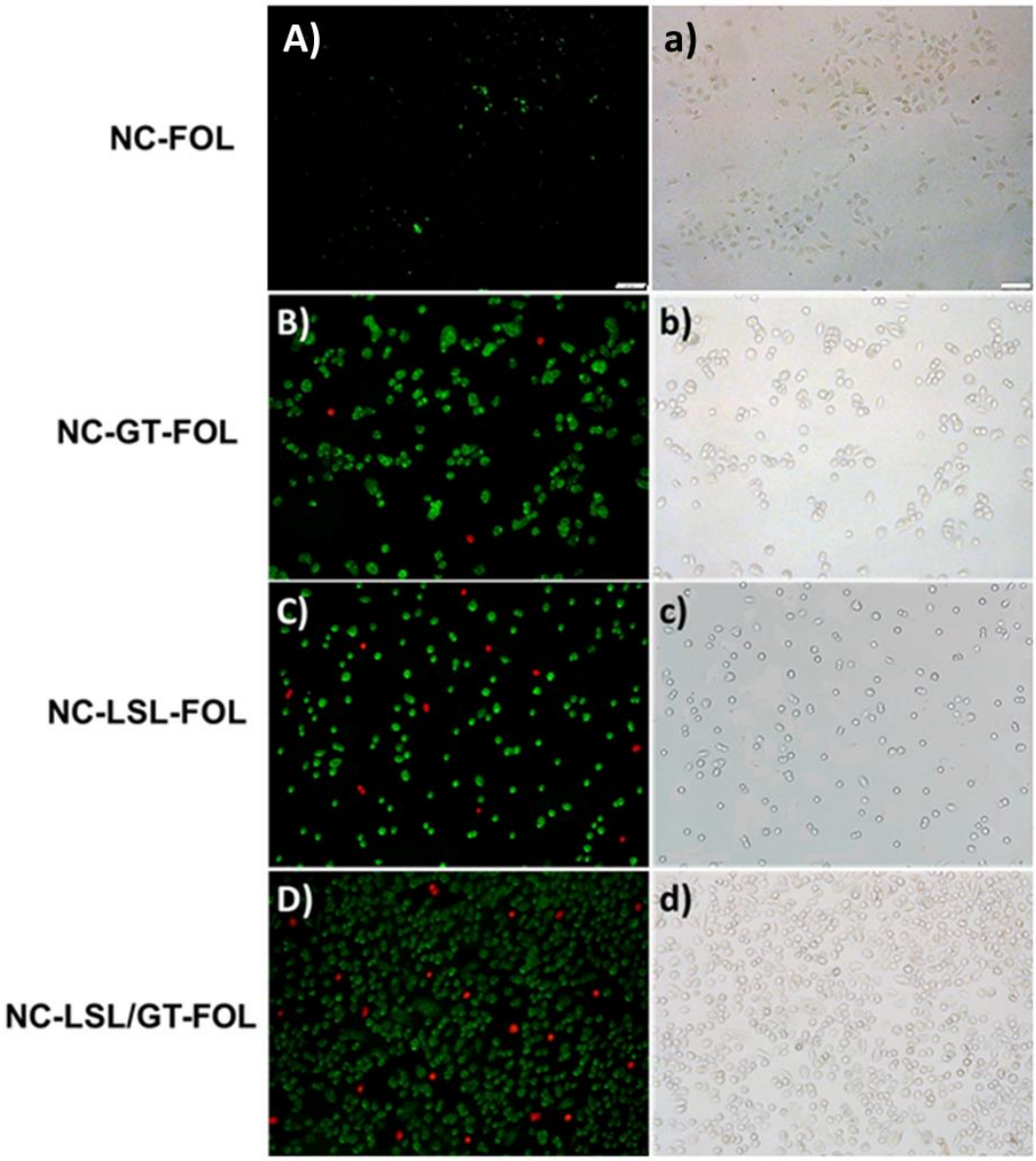

Figure 9: Detection of apoptotic and necrotic cell death by fluorescence microcopy using annexin V-FITC and ethidium homodimer III. (A) Healthy cells emitted limited fluorescence representing early apoptosis. (B & C) When incubated with single drugs, green fluorescence was emitted by apoptotic cells (D) Combinational drugs exhibited both green and red fluorescence due to late apoptotic and necrotic cells. (a, b, c and d) represents corresponding bright field images.

Migration assay:

Metastasis is the deadliest aspect of cancer and remains the principal cause of death despite of research aimed at restricting tumor growth. One such case is with K-RAS driven NSCLC. To assess whether our combinational drugs carrying nanoceria is capable of inhibiting the migration of tumor cells; we performed transwell migration assays. Briefly, in these experiments, A549 cells were serum starved and treated with functional nanoparticles (1.0 X 10^{-3} mol) and incubated for 24 h by seeding in upper invasion chamber. When incubated with only nanoceria (no drugs, NC-FOL) our results showed that the cells migrated from invasion chamber to the lower feeder tray containing 10% FBS **(**CTRL, **Figure 10)**. However, upon incubation with combinational drugs, the migration ability of cells has decreased considerably as noticed by the change in fluorescence intensity **(Figure 10)**. Collectively, our results demonstrated that the combinational drug therapy of LSL and GT along with the functional nanoceria might play an important role in preventing the metastatic nature of NSCLC.

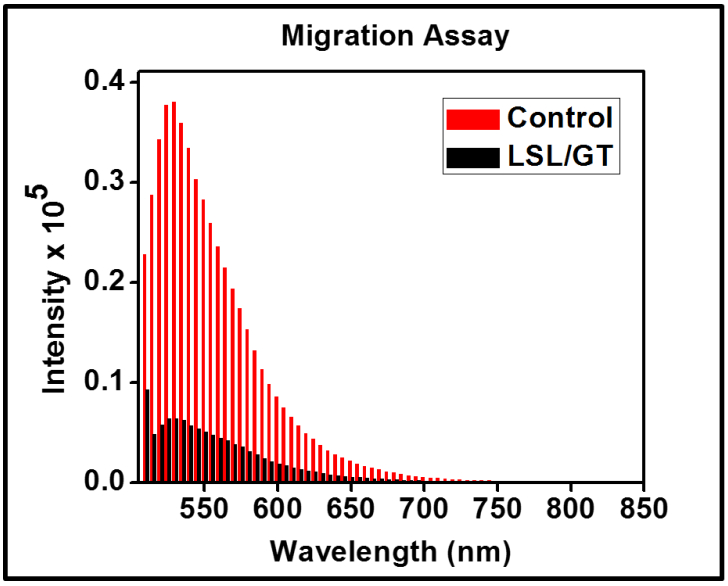

Figure 10: Determination of anti-migratory effect of highly metastatic lung cancer cells via migration assay. As represented, control (no drugs, red lines) showed significant migration of cells. Whereas, nanoceria with combinational drug (black lines) had showed minimal migration as the drugs are capable of inhibiting the metastatic nature of the cells.

HDAC Inhibition assay:

For the detection of HDAC inhibition activity of lactonic sophorolipids, we performed the fluorescent HDAC inhibition assay according to manufacturer protocol. As presented **(Figure 11)**, positive control (HeLa extract, has HDAC activity) has shown high fluorescence intensity as the substrate containing acetylated lysine residue is deacetylated by the HDAC enzyme. In contrast, negative control, Trichostatin had shown minimum fluorescence as the HDAC is completely inhibited and therefore the acetylated residue is not deacetylated. When incubated with our functional nanoparticles (NC-LSL/GT-FOL and NC-LSL-FOL), significant fluorescence was seen as the acetylated HDAC substrate is not deacetylated due to the HDAC inhibition. As a result, there is a reduction in fluorophore intensity in the sample wells (low fluorescence intensity), when

compared to positive control thereby confirming that lactonic sophorolipids follows the HDAC inhibition pathway leading to the apoptosis. However, ganetespib, the combinational drug of LSL in our study is showing a modest synergistic effect during this mechanism.

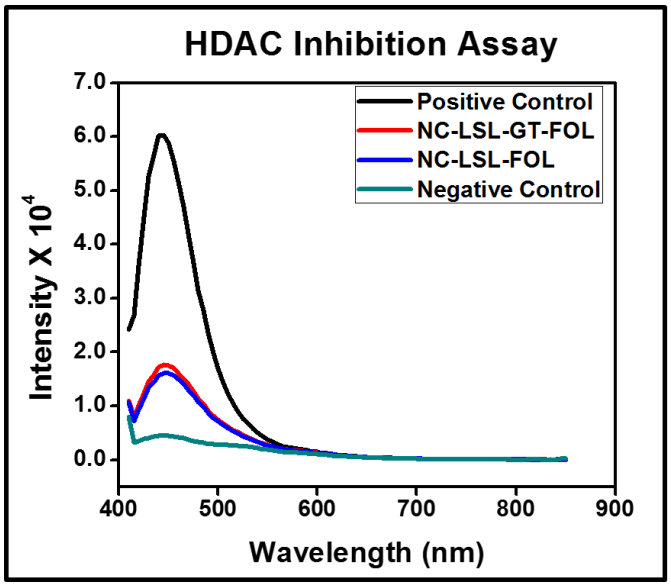

Figure 11: Assessment of inhibition of histone deacetylase (HDAC) by lactonic sophorolipids (LSL) in comparison with positive and negative controls. As depicted, positive control shows enormous inhibition and the drugs had significant effect on HDAC inhibition with that of negative control.

CHAPTER III

Experimental Methods

Materials:

Cerium nitrate hexahydrate ($Ce(NO_3)_3$), Polyacrylic acid (PAA), Ammonium hydroxide (NH_4OH), Folic acid, N-hydroxysuccinimide (NHS), 2(N—morpholino) ethanesulfonic acid (MES) sodium salt, Tetrahydron furan, acetonitrile, Sodium azide, Ethanol, Isopropanol and Propargylamine (PA) were purchased from Acros organics and used without further purification. Near infrared dye (DiI-D282) was obtained from Life technologies. N, N'-dimethyl formamide (DMF) and Dihydroethidium (DHE) dye was purchased from Science lab and Cayman chemicals respectively. N, N'-dimethyl sulfoxide (DMSO), 3-(4, 5-dimethylthiazol-2-yl) - 2, 5-diphenyltetrazolium bromide (MTT) and (1-ethyl-3-[3-(dimethylamino) propyl] carbodiimide hydrochloride) (EDC) were obtained from Sigma Aldrich and used as received. 4, 6-diamidino-2-phenylindole (DAPI-D1306) was purchased from Invitrogen. Dialysis membrane were received from spectrum laboratories. Paraformaldehyde and H_2O_2 were received from electron microscopy sciences. Fetal bovine serum (FBS) and 5X Annexin binding buffer were purchased from BD biosciences, whereas Gantespib, Isopropyl alcohol, Apoptosis and Necrosis quantification kit (FITC-Annexin V, Ethidium homodimer III) were obtained from Biotium. Migration assay kit and HDAC inhibition fluorometric assay kit was obtained from Millipore

and Biovision respectively. The human lung carcinoma cell line A549 cells (NSCLC) and Chinese hamster cells (CHO) were obtained from ATCC (U.S.A). Dulbecco's modified eagle (DMEM) medium and Kaighn's modification of Ham's F12K cell culture medium were purchased from Corning.

Synthesis of Poly (acrylic acid)-Coated Nanoceria (NC-COOH) (1):

To synthesize PAA coated nanoceria, previously reported alkaline-based precipitation method was followed, where the cerium oxide nanoparticles were precipitated from a solution of ammonium hydroxide containing cerium salt and PAA. The synthetic procedure involves the preparation of two different solutions – Solution A: cerium nitrate (0.9 g) in 2.5 ml of DI water, Solution B: PAA (0.9 g) in 10 ml of DI water. 30 ml of ammonium hydroxide was taken in a beaker and was stirred at room temperature and solution A was added to it followed by addition of solution B. We can notice the color change from colorless to brown within 5 min of stirring and became deep yellow after 24 h, indicating the preparation of stable nanoceria. The reaction mixture was centrifuged thrice at 3000, 3500 and 4000 rpm for 15, 20 and 20 min respectively to obtain smaller size nanoparticles. The solution was further purified by dialysis technique using a dialysis bag of molecular weight (MWCO) 6-8K against DI water and finally with phosphate buffer saline (PBS, pH = 7.4) to remove ammonium hydroxide by selective and passive diffusion through a semi-permeable membrane (dialysis tubing) (Scheme 1). The purified nanoceria was stored at 4°C for further characterizations. Successful coating of PAA on nanoceria was characterized by Fourier Transform Infra-Red (FT-IR) spectroscopy. Overall size and surface charge were measured using dynamic light scattering (DLS) technique.

Synthesis of propargylated or alkynated NC (3); Carbodiimide chemistry:

Propargylated NC was synthesized by adding freshly prepared EDC (15 X 10^{-3} mol) solution followed by addition of NHS (15 X 10^{-3} mol) in 200 µL of MES buffer (0.1 M), pH = 6.0, after brief mixing. The reaction mixture was incubated for an additional 3 min at room temperature and then propargylamine (15 X 10^{-3} mol) dissolved in DMSO was added dropwise and mixed. The reaction was continued for 4-6 h for completion at room temperature. The resultant propargylated NC was purified against PBS (pH = 7.4) using the dialysis method to remove the unreacted reagents from the solution.

Synthesis of Aminopropyl azide:

Aminopropylazide was synthesized by reacting chloropropyl amine (7.0 g, 75.26 mmol) and sodium azide (14.23 g, 225.81 mmol) in 40 mL of distilled water. The reaction was carried out at 800 C for 20 h. The reaction mixture is then concentrated using rotary evaporator at high vacuum. 2 g of KOH was added and the product was extracted using diethyl ether. Subsequently, the reaction mixture was dried over anhydrous sodium sulfate and concentrated. Purification of the product was done by column chromatography using 4% ethyl acetate in petroleum ether.

Synthesis of folate-azide; Carbodiimide chemistry:

To the solution of folic acid (0.05 g, 0.12 mmol) in 7 mL phosphate buffer saline (PBS, pH 7.4), freshly prepared EDC (0.021 g, 0.11 mmol) followed by NHS (0.013 g, 0.11mmol) in 0.25 mL MES buffer (pH = 5.0) were added and then incubated at room temperature for about 3. To this resulting mixture, add dropwise aminopropyl azide (0.0014 g, 0.11 mmol) in 0.5 mL of MES (pH = 5.0) and incubate it for 3 h at room temperature. The carboxyl groups of folic acid react with azide and forms azide-functionalized folic acid.

Synthesis of folate conjugated NC (NC-FOL) (4 and 5) using "click chemistry":

To the solution of alkynated NC suspension (2 mL, 1.5 X 10^{-3} mmol) in bicarbonate buffer (pH 7.4) and folate-azide (FoL~N3, 2 X 10^{-2} mol), catalytic amount of CuI catalyst (1 X 10-3 mmol) in DMF was added and incubated on table mixer for overnight at room temperature. The resulting folate conjugated NC was purified by dialysis to remove unreacted materials. The purified product was stored at 4°C for further characterizations.

Encapsulation of DiI dye (2 and 4): Modified solvent diffusion method:

For dye encapsulation, solvent diffusion method has been used. To 1 mL of nanoceria (NC-COOH or NC-FOL) suspension, near infrared DiI dye (1 µL of 1 µM DiI dye in 100 µL of DMSO) was added dropwise with continuous stirring at 1500 rpm at room temperature. The solution was incubated on table-mixer for 3 h and was dialyzed against PBS (pH = 7.4) for 2 h to remove free dye from the solution. Successful encapsulation of DiI was further confirmed using UV-Vis and fluorescence spectrophotometric analyses. The purified dye-labeled nanoceria was stored at 4°C for further studies.

Coencapsulation of Lactonic sophorolipids (LSL), Ganetespib (GT):

Using a similar solvent diffusion method, drug or combination of drugs and dye were co-encapsulated. Briefly, a solution of either LSL and DiI or LSL-GT-DiI or GT and DiI (2 µM of the drug in 100 µL DMSO) was added dropwise to 2 mL of vortexing NC-FOL suspension, followed by overnight incubation. The drug-encapsulating functional NC-FOL were dialyzed against PBS (pH = 7.4) for 3 h. The purified suspension was stored at 4°C for further characterizations. The presence of DiI dye was confirmed by using US-Vis and fluorescence spectrophotometry.

Characterizations of Functional Nanoceria:

Fourier transform infrared spectroscopy (FTIR):

To verify the surface functionalities of our synthesized nanoceria, we performed FTIR studies using Perkin-Elmer's Spectrum. PAA coated nanoceria was air dried and the powdered crystals were collected. FT-IR spectra of dried PAA coated nanoceria and PAA polymer was recorded and compared to confirm the successful coating of PAA on the synthesized nanoparticles.

Dynamic light scattering (DLS):

The average size distribution and surface charge of the functional nanoceria were obtained using dynamic light scattering technique. Malvern's nano-ZS90 zeta sizer was used for DLS studies.1 ml of NC-COOH was taken in the cuvette and measured for size using standard procedure set in Malvern Zetasizer. For measuring zeta potential, the sample was diluted with DI water and is carefully loaded in electrode without air bubble and the zeta potential is measured and recorded.

Spectrophotometric analysis:

UV-vis and fluorescence spectroscopic studies of functional nanoceria were recorded using TECAN's infinite M200 PRO high throughput plate reader to confirm the successful conjugation of folic acid ligands on the surface of nanoceria for targeted drug delivery. Similarly, the studies were also performed for the presence of DiI dye in the nanoparticles for optical imaging. The procedure involves the addition of 75 µL of suspension in Thermo Fisher 96 well plate and measuring the absorbance and fluorescence at 300-800 nm and 585 nm wavelengths respectively.

***In vitro* cell studies:**

Cell Culture:

Human lung cancer cells (A549 cells) and Chinese Hamster ovarian cells (CHO cells – normal cells) were obtained from ATCC. A549 cells were maintained in a 10% FBS-containing DMEM medium supplemented with 1% antibiotic, whereas, CHO cells were propagated in 10% FBS containing Ham's F12K media containing 1% penicillin-streptomycin antibiotic. Cells were grown under 5% CO2 atmosphere at 37° C in a humidified incubator.

Cell viability assay (MTT Assay):

To determine the time-dependent cytotoxicity, two different cell lines, lung carcinoma (A549 cells) and Chinese hamster ovarian cells (CHO cells) were used. Cells were seeded in 96-well plates at a density of 3500 cells per well and treated with various functional folate conjugated nanoceria (1.0×10^{-3} mol) and incubated at 37° C for different time points. Each well was washed twice with PBS and then incubated with 30 µL of 5mM MTT solution. After 4-6 h of incubation, the resulting formazan crystals (purple color) were dissolved in acidic isopropanol (75 µL) and the absorbance was recorded at 570 nm using TECAN's microplate reader. The assay was carried out in triplicates and the results are reported.

Drug release profiles:

The in vitro dye/drug release studies were carried out by using a dynamic dialysis technique at 37° C. Drug/dye-loaded nanoparticles were packed in a dialysis bag and suspended in 2 different environments of PBS (200 mL, pH 7.4 and 6). The amount of drug/dye molecules released from the nanoparticles into the PBS solution was

determined at regular intervals of time by taking 1 mL aliquots from the PBS solution and replacing the same with PBS solution. Fluorescence emission was measured at 585 nm for DiI dye. The concentration of dye released was calculated using standard calibration curve and the cumulative release versus time was calculated using the following equation:

$$\text{Cumulative release (\%)} = (\text{dye released})_t / (\text{dye released})_{total} \times 100$$

Where, $(\text{dye released})_t$ is the amount of dye released at time t, and $(\text{dye released})_{total}$ is the total dye present in the dye/drug encapsulated nanoparticles.

Confocal Laser-Scanning Microscopy:

Lung carcinoma cells (A549 cells) and Chinese Hamster Ovarian cells (CHO – Normal cells) were seeded into the culture dishes and grown overnight. Once the cells are 75% confluent, different functional drug loaded nanoparticles (NC-COOH, NC-DiI-FOL, NC-LSL-GT-DiI-FOL, 1.0 X 10^{-3} mol) were treated to the cells and incubated at 37° C for 24 h. The cells were washed thrice with 1X PBS (pH = 7.4) and were fixed with 4% formaldehyde solution for 15 min at room temperature. The cells were again washed with 1X PBS before treating with DAPI dye (5mg/mL) for staining cell nuclei. The cells were then washed with 1X PBS and optical images were taken using fluorescence microscope (Olympus IX73) for cellular internalization of dyes and killing of cells. For the control experiment, CHO cells were treated with NC-LSL-GT-DiI-FOL (1.0 X 10^{-3} mol) and the results were shown.

Cytosolic ROS detection assay:

To know the mechanism of the killing process of cancerous cells, various assays were performed, of which, ROS is one among them. This assay determines the process of induction of stress to the cells by the generation of reactive oxygen species. A549 cells

were seeded in 12-well plates at a density of 10000 cells per well and treated with nanoparticles encapsulated with different drugs (1.0 X 10^{-3} mol) and incubated at 37° C. After 6 h of incubation, the cells were washed thrice with 1X PBS and stained with 20 µL of DHE fluorescent probe for about 30min at room temperature followed by washing the cells twice with 1X PBS. Subsequently, the cells were fixed with 1 mL of paraformaldehyde solution. After fixation, the cells were washed with 1X PBS, stored with 2 mL PBS in each well and optical images were taken using fluorescence microscope.

Quantification of ROS fluorescent images:

Using ROS fluorescent images, the amount of ROS was quantified using commercial ImageJ software. Particular cell from each treated well was selected to get a stack of values for the area, integrated density, and mean fluorescence of background readings. The corrected total cell fluorescence (CTCF) for each well was calculated using the formula:

CTCF = integrated density – (area of selected cell X mean fluorescence of background readings).

Apoptosis and necrosis detection assay:

For the assessment of apoptosis and necrosis, Annexin V-FITC and Ethidium homodimer III was used. This assay is based on the translocation of phosphatidylserine (PS) from the plasma membrane to the cell surface soon after the initiation of apoptosis. The translocated PS can be easily detected by a protein, Annexin V in conjugation with FITC which has the strong affinity for PS. Briefly, A549 cells were seeded in 12-well plates at a density of 10000 cells per well. After confluence, cells were treated with different preparations (NC-FOL, NC-LSL-FOL, NC-GT-FOL and NC-LSL-GT-FOL, 1.0 X 10^{-3} mol).

After 6 h of incubation, the cells were washed twice with 1X PBS and stained with two different dyes, 5 µL of FITC-annexin buffer and 5 µL of ethidium homodimer III and incubated for 15 min in the dark. Later the cells were washed twice with 1X binding buffer and fixed with 4% formaldehyde solution and the cells were covered with 1X binding buffer. Multiple fluorescence images were taken using two filters: green fluorescence represents apoptosis; red fluorescence indicates necrosis.

Migration Assay:

Cell migration is a multi-step process that plays an important role in the progression of cancer and other diseases. It is the movement of cells from one area to another in response to a chemical signal. Currently, determining the migratory and invasive capacity of tumor cells and elucidating their mechanisms is more important for cancer diagnosis and treatment. Herein Chemicon QCM 96-well cell migration assay kit from Millipore was used to evaluate the migration of cells in presence of functional nanoparticles in vitro. Experimental procedure involves the incubation of serum starved A549 cells for 24 h. Next, the cells were harvested and treated with the functional nanoparticles (NC-LSL/GT-FOL). Subsequently, the cells were seeded in invasion chamber of the migratory assay kit coated with collagen layer. The feeder tray contained 10% FBS media and the complete set up was incubated at 37° C for 24 h to allow the migration of cells. Later, the migratory cells were dislodged completely from the invasion chamber and placed on new feeder tray containing cell detachment buffer and incubated for 30 min. Finally, a diluted solution of CyQuant GR dye and cell lysis buffer was added to stain migratory cells and the fluorescence intensity was measured at an emission wavelength of 480/520 nm.

HDAC Inhibition Assay:

Acetylation and deacetylation of histone proteins influence the gene expression by modulating the chromatin structure. Two enzymes, histone acetyltransferase (HAT) and histone deacetylase (HDAC) mediate the balance between acetylated and deacetylated states. HDAC has a wide spectrum of cellular functions including regulation of gene transcription, translocation of transcriptional factors and apoptosis by altering acetylation of various proteins. Several studies have shown that inhibiting HDAC in cancer cells leads to cell differentiation and reduced cell growth, making HDAC notable and attractive antitumor target for cancer therapy.

HDAC fluorometric assay kit from Biovision was used to determine the HDAC inhibition ability of lactonic sophorolipids (LSL). The assay was performed according to manufacturer's protocol. HeLa nuclear extract and Trichostatin A were used as positive and negative controls respectively. Briefly, A549 cells were seeded in 96-well microtiter plates (10000 cells/well) and after 80% confluence, the cells were treated with nanoparticles (NC-LSL/GT-FOL and NC-LSL-FOL) and incubated at 37° C for 24 h. Positive and negative controls were added along with HDAC assay buffer and the reaction was initiated by adding HDAC fluorometric substrate and incubating for 30 min or longer as desired by the drugs. Later, the HDAC lysine developer was added to stop the reaction and is incubated for additional 15 min. The plate is then read for fluorescence intensity at 380/460 nm.

CHAPTER IV

Conclusions

In conclusion, we have successfully synthesized functional nanoceria with combinational drugs as a drug vehicle for the treatment of K-RAS driven NSCLC. Targeted delivery is achieved through folate conjugation of nanoceria and the synergistic effect of combinational drugs was observed. Encapsulation studies and enhanced stability confirmed excellent drug payload with high therapeutic efficacy and reduced toxicity. More than 90% of cells were dead when incubated with combinational drugs as reflected by combinational therapy. Results indicated that GT synergizes the activity of LSL, as confirmed by MTT and ROS assays. Apoptosis and necrosis assays further proved the synergistic effect of drugs by increased apoptotic and necrotic cells. In addition, migration assay validated the important role of combinational drugs in preventing lung cancer metastasis. Therefore, our study of delivering combinational drugs using functional nanoceria provides clinically actionable information that could impact treatment decisions for individuals with K-RAS driven NSCLC.

REFERENCES

1. Ropero, S.; Esteller, M. The role of histone deacetylases (HDACs) in human cancer. Mol. Oncol. **2007**, 1, 19-25.
2. He, S.; Smith, D. L.; Sequeira, M.; Sang, J.; Bates, R. C.; Proia, D. A. The HSP90 inhibitor ganetespib has chemosensitizer and radiosensitizer activity in colorectal cancer. Invest. New Drugs **2014**, 32, 577–586.
3. Peserico, A.; Simone, C. Physical and functional HAT/HDAC interplay regulates protein acetylation balance. J. Biomed. Biotechnol. **2011**, Article No. 371832.
4. Chen, H. P.; Zhao, Y. T.; Zhao, T. C. Histone deacetylases and mechanisms of regulation of gene expression (Histone deacetylases in cancer). Crit Rev Oncog. **2015**, 20(1-2), 35–47.
5. Annemieke, J. M.; Ruijter, D.; Gennip, A. H. V.; Caron, H. N.; Kemp, S.; Kuilenburg, A. B. P. V. Histone deacetylases (HDACs): Characterization of the classical HDAC family. Biochem. J. **2003**, 370, 737–749.
6. Bali, P.; Pranpat, M.; Bradner, J.; Balasis, M.; Fiskus, W.; Guo, F.; Rocha, K.; Kumaraswamy, S.; Boyapalle, S.; Atadja, P.; Seto, E.; Bhalla, K. Inhibition of histone deacetylase 6 acetylates and disrupts the chaperone function of heat shock protein 90. J. Biol. Chem. **2005**, 22, 26729–26734.

7. New, M.; Olzscha, H.; Thangue, N. B. HDAC-inhibitor based therapies: Can we interpret the code? Mol. Oncol. **2012**, 6, 637-656.
8. Johnstone, R. W. Histone-deacetylase inhibitors: Novel drugs for the treatment of cancer. Nat. Rev. Drug Discov. **2002**, 4, 287-299.
9. Bode, K. A.; Schroder, K.; Hume, D. A.; Ravasi, T.; Heeg, K.; Sweet, M. J.; Dalpke, A. H. Histone deacetylase inhibitors decrease Toll-like receptor-mediated activation of proinflammatory gene expression by impairing transcription factor recruitment. Immunology **2007**, 122, 596–606.
10. Hull, E. E.; Montgomery, R.; Leyva, K. J. HDAC inhibitors as epigenetic regulators of the immune system: Impacts on cancer therapy and inflammatory diseases. Biomed. Res. Int. **2016**, Article No. 8797206.
11. Glaser, K. B.; Staver, M. J.; Warning, J. F.; Ulrich, J. S. R. G.; Davidsen, S. K. Gene expression profiling of multiple histone deacetylase (HDAC) inhibitors: Defining a common gene set produced by HDAC inhibiton in T24 and MDA carcinoma cell lines. Mol. Cancer Ther. **2003**, 2, 151–163.
12. Yang, X. J.; Seto, E. HATs and HDACs: From structure, function and regulation to novel strategies for therapy and prevention. Oncogene **2007**, 26, 5310–5318.
13. Xu, W.S.; Parmigiani, R. B.; Marks, P. A. Histone deacetylase inhibitors: Molecular mechanisms of action. Oncogene **2007**, 26, 5541–5552.
14. Kurtzman, C. P.; Price, N. P. J.; Ray, K. J.; Kuo, T. Production of sophorolipid biosurfactants by multiple species of the Starmerella (Candida) bombicola yeastclade. FEMS Microbiol. Lett. **201,** 311, 140–146.

15. Oliveira, M. R.; Camilios-Neto, D.; Baldo, C.; Magri, A.; Celligoi, M. A. P. C. Biosynthesis and Production of Sophorolipids. Int. J. Sci. Tech. Res. **2014**, 11, 133-146.
16. Hardin, R.; Pierre, J.; Schulze, R.; Mueller, C. M.; Fu, S. L.; Wallner, S. R.; Stanek, A.; Shah, V.; Gross, R. A.; Weedon, J.; Nowakowski, M.; Zenilman, M. E.; Bluth, M. H. Sophorolipids improve sepsis survival: Effects of dosing and derivatives. J. Surg. Res. **2007**, 142, 314-319.
17. Sleiman, J. N.; Kohlhoff, S. A.; Roblin, P. M.; Wallner, S.; Gross, R.; Hammerschlag, M. R.; Zenilman, M. E.; Bluth, M. H. Sophorolipids as antibacterial agents. Ann. Clin. Lab. Sci. **2009**, 39, 60-63.
18. Oliveira, M. R.; Magri, A.; Baldo, C.; Camilios-Neto, D., Minucelli, T.; Celligoi, M. A. P. C. Review: Sophorolipids A promising biosurfactant and its applications. Intl. J. of Adv. Biotec. and Res. **2015**, 6, 161-174.
19. Callaghan, B.; Lydon, H.; Roelants, S. L. K. W.; Marchant, I. V. B. R.; Banat, I. M.; Mitchell, C. A. Lactonic sophorolipids increase tumor burden in Apcmin+/- mice. PLoS One **2016**, 11, e0156845.
20. Rashad, M.M.; Nooman, M.U.; Ali, M.M.; Al-kashef A.S.; Mahmoud, A.E. Production, characterization and anticancer activity of Candida bombicola sophorolipids by means of solid state fermentation of sunflower oil cake and soybean oil. Grasas Aceites. **2014**, 65, e017.
21. Marks, P. A. The clinical development of histone deacetylase inhibitors as targeted anticancer drugs. Expert Opin. Investig. Drugs **2010,** 19, 1049–1066.

22. Li, H.; Guo, W.; Ma, X.; Li, J.; Song, X. In Vitro and In Vivo anticancer activity of sophorolipids to human cervical cancer. Appl. Biochem. and Biotechnol. **2016**, 1-16
23. Shao, L.; Song, X.; Ma, X.; Qu, Y. Bioactivities of sophorolipids with different structures against human esophageal cancer cells. J. Surg. Res. **2010**, 173, 286-291.
24. Fu, S. L.; Wallner, S. R.; Bowne, W. B.; Hagler, M. D.; Zenilman, M. E.; Gross, R.; Bluth, M. H. Sophorolipids and their derivatives are lethal against human pancreatic cancer cells. J. Surg. Res. **2008,** 148, 77–82.
25. Joshi-Navare, K.; Shiras, A.; Prabhune, A. Differentiation-inducing ability of sophorolipids of oleic and linoleic acids using a glioma cell line. J. Biotechnol. **2011**, 6, 509–512.
26. Ribeiro, I. A.; Faustino, C. M.; Guerreiro, P. S.; Frade, R. F.; Bronze, M. R.; Castro, M. F.; Ribeiro, M. H. Development of novel sophorolipids with improved cytotoxic activity toward MDA-MB-231 breast cancer cells. J. Mol. Recognit. **2015**, 28, 155–165.
27. Molina, J. R.; Yang, P.; Cassivi, S. D.; Schild, S. E.; Adjei, A. A. Non–Small cell lung cancer: Epidemiology, risk factors, treatment, and survivorship. Mayo Clin Proc. **2008**, 83, 584–594.
28. Sukumar, U. K.; Bhushan, B.; Dubey, P.; Matai, I.; Sachdev, A.; Pakirisamy, G. Emerging applications of nanoparticles for lung cancer diagnosis and therapy. Int. Nano Lett. **2013**, 3, 45.

29. Sadhukhaa, T.; Wiedmanna, T. S.; Panyam, J. Inhalable magnetic nanoparticles for targeted hyperthermia in lung cancer therapy. Biomaterials **2013**, 34, 5163–5171.
30. Oser, M. G.; Niederst, M. J.; Sequist, L. V.; Engelman, J. A. Transformation from non-small-cell lung cancer to small-cell lung cancer: molecular drivers and cells of origin. Lancet Oncol. **2015**, 16, 165–172.
31. Ahmad, J.; Akhter, S.; Rizwanullah, M.; Amin, S.; Rahman, M.; Ahmad, M. Z.; Rizvi, M. A.; Kamal, M. A.; Ahmad, F. J. Nanotechnology-based inhalation treatments for lung cancer: State of the art. Nanotechnol. Sci. and Appl. **2015**, 8, 55–66.
32. Munaweera, I.; Shi, Y.; Koneru, B.; Saez, R.; Aliev, A.; Pasqua, A. J. Balkus, K. J. Chemoradiotherapeutic magnetic nanoparticles for targeted treatment of Nonsmall cell lung cancer. Mol. Pharmaceutics **2015**, 12, 3588−3596.
33. Ramalingam, S. S.; Owonikoko, T. K.; Khuri, F. R. Lung cancer: New biological insights and recent therapeutic advances. CA Cancer J Clin. **2011**, 61, 91–112.
34. Jemal, A.; Bray, F.; Center, M. M.; Ferlay, J.; Ward, E.; Forman, D. Global cancer statistics. CA Cancer J Clin. **2011**, 61, 69–90.
35. Shen, S.; Mao, C.; Yang, X.; Du, X.; Liu, Y.; Zhu, Y.; Wang, J. Cationic lipid-assisted polymeric nanoparticle mediated GATA2 siRNA delivery for synthetic lethal therapy of KRAS mutant Non-small-cell lung carcinoma. Mol. Pharmaceutics **2014**, 11, 2612−2622.

36. Westcott, P. M. K.; To, M. D. The genetics and biology of K-RAS in lung cancer. Chin. J. Cancer **2013**, 32, 63-70.
37. D'Arcangelo, M.; Cappuzzo, F. K-Ras mutations in Non-small-cell lung cancer: Prognostic and predictive value. ISRN Mol. Biol. 2012, Article No. 837306.
38. Ramalingam, S.; Belani, C. Systemic chemotherapy for advanced non-small cell lung cancer: recent advances and future directions. Oncologist **2008**, 13 (Suppl1), 5−13.
39. Grossi, F.; Kubota, K.; Cappuzzo, F.; De Marinis, F.; Gridelli, C.; Aita, M.; Douillard, J. Y. Future scenarios for the treatment of nonsmall cell lung cancer: Focus on taxane-containing regimens. Oncologist **2010**, 15, 1102−1112.
40. Jhaveri, K.; Modi, S. Ganetespib: Research and clinical development. OncoTargets and Ther. **2015**, 8, 1849–1858.
41. Tsutsumi, S.; Beebe, K.; Neckers, L. Impact of heat-shock protein 90 on cancer metastasis. Future Oncol. **2009**, 5, 679–688.
42. Lia, Y.; Zhanga, T.; Sun, D. New developments in Hsp90 inhibitors as anti-cancer therapeutics: Mechanisms, clinical perspective and more potential. Drug Resist Updat. **2009**, 12, 17–27.
43. Shimamura T.; Shapiro, G. I. Heat shock protein 90 inhibition in lung cancer. J. Thorac. Oncol. **2008**, 3, 602.
44. Beck, R.; Dejeans, N.; Glorieux, C.; Pedrosa, R. C.; Vásquez, D.; Valderrama, J. A.; Calderon, P. B.; Verrax, J. Molecular chaperone Hsp90

as a target for oxidant-based anticancer therapies. Curr. Med. Chem. **2011**, 18, 1-10.

45. Rios, D.; Benites, J.; Valderrama, J. A.; Farias, M.; Pedrosa, R. C.; Verrax. J.; Calderon, P. B. Biological evaluation of 3-acyl-2-acrylamino-1, 4-napthaquinones as inhibitors of Hsp90 chaperoning function. Curr. Top. Med. Chem. **2012**, 12, 2094-2102.
46. He, S.; Smith, D. L.; Sequeira, M.; Sang, J.; Bates, R. C.; Proia, D. A. The HSP90 inhibitor ganetespib has chemosensitizer and radiosensitizer activity in colorectal cancer. Invest. New Drugs. **2014**. 32, 577–586.
47. Sulthana, S.; Banerjee, T.; Kallu, J.; Reddy, S. V; Heckert, B.; Naz, S.; Shelby, T.; Yambem, O.; Santra, S. Combination Therapy of NSCLC Using HSP90 Inhibitor and Doxorubicin carrying Functional Nanoceria. Mol. Pharm. **2017,** 14, 875-884.
48. Jabir, N. R.; Tabrez, S.; Ashraf, G. M.; Shakil, S.; Damanhouri, G. A.; Kamal, M. A. Nanotechnology-based approaches in anticancer research. Int. J. Nanomedicine. **2012**, 7, 4391-4408.
49. Calixto, G.; Bernegossi, J.; Fonseca-Santos, B.; Chorilli, M. Int. J. Nanomedicine. **2014**, 9, 3719-3735.
50. Qureshi, S. R.; Sahni, Y. P.; Singh, S. K.; Bhat, M. A.; Dara, A. A.; Quadri, S. A. Nanotechnology based Drug Delivery System. J. Pharm. Res. Opinion. **2011,** 1, 6, 161-165.
51. McNeil, S.E. Unique benefits of nanotechnology to drug delivery and diagnostics. Methods Mol. Biol. **2011**, 697, 3–8.

52. Bawarski, W. E.; Chidlowsky, E.; Bharali, D.J.; Mousa, S. A. Emerging Nanopharmaceuticals. Nanomedicine. **2008**, 4, 273–282.

53. Zhang, L. Gu, F. X.; Chan, J. M.; Wang, A. Z.; Langer, R. S.; Faraokhzad, O. C. Nanoparticles in medicine: Therapeutic applications and developments. Clin. Pharmacol. Ther. **2008**, 83, 761–769.

54. Piktel, E.; Niemirowicz, K.; Watek, M.; Wollny, T.; Deptula, P.; Bucki R. Recent insights in nanotechnology-based drugs and formulations designed for effective anti-cancer therapy. J. Nanobiotechnol. **2016**, 14, 39.

55. Safari, J.; Zarnegar, Z. Advanced drug delivery systems: Nanotechnology of health design A Review. J. Saudi Chem. Soc. **2014,** 18, 85-99.

56. Thakor, A. S.; Gambhir, S. S. Nanooncology: The future of cancer diagnosis and therapy. CA Cancer J. Clin. **2013,** 63, 395–418.

57. Vieira, D. B.; Gamarra, L. F. Advances in the use of nanocarriers for cancer diagnosis and treatment. Einstein **2016**, 14, 99-103.

58. Xu, C.; Qu, X.; Cerium oxide nanoparticle: A remarkably versatile rare earth nanomaterial for biological applications. NPG Asia Materials **2014**, 6, e90.

59. Pulido-Reyes, G.; Rodea-Palomares, I.; Das, S.; Sakthivel, T. S.; Leganes, F.; Rosal, R.; Seal, S.; Fernández-Piñas, F. Untangling the biological effects of cerium oxide nanoparticles: The role of surface valence states. Scientific Reports **2015**, 5, 15613.

60. Nelson, B. C.; Johnson, M. E.; Walker, M. L.; Riley, K. R.; Sims, C. M. Antioxidant cerium oxide nanoparticles in biology and medicine. Antioxidants (Basel). **2016**, 5, 15.

61. Giri, S.; Karakoti, A.; Graham, R. P.; Maguire, J. L.; Reilly, C. M.; Seal, S.; Rattan, R.; Shridhar, V. Nanoceria: A Rare-earth nanoparticle as a novel anti angiogenic therapeutic agent in ovarian cancer. PLoS One **2013**, 8, e54578.
62. Dowding, J. M.; Das, S.; Kumar, A.; Dosani, T.; McCormack, R.; Gupta, A.; Sayle, T. X. T.; Sayle, D. C.; Kalm, L. V.; Seal, S.; Self, W. T. Cellular interaction and toxicity depend on physicochemical properties and surface modification of redox-active nanomaterials. ACS Nano **2013**, 7, 4855–4868.
63. Sack, M.; Alili, L.; Karaman, E.; Das, S.; Gupta, A.; Seal, S.; Brenneisen, P. Combination of conventional chemotherapeutics with redox-active cerium oxide nanoparticles—A novel aspect in cancer therapy. Mol Cancer Ther. **2014**, 13, 1740-1749.
64. Nguyen, A.; Su, L.; Campbell, B.; Poulin, N. M.; Nielsen, T. O. Synergism of heat shock protein 90 and histone deacetylase inhibitors in synovial sarcoma. Sarcoma **2009**, Article No. 79490.
65. Kramer, O. H.; Mahboobi, S.; Sellmer, A. Drugging the HDAC-HSP90 interplay in malignant cells. Trends in Pharmacol. Sci. **2014**, 35, 501-509.
66. Perez, J. M.; Asati, A.; Nath, S.; Kaittanis, C. Synthesis of biocompatible dextran-coated nanoceria with pH-dependent antioxidant properties. Small **2008**, 4, 552-556.
67. Asati, A.; Santra, S.; Kaittanis, C.; Perez, J. M. Surface-charge-dependent cell localization and cytotoxicity of cerium oxide nanoparticles. ACS Nano **2010**, 4, 5321-5331.